Electronic Supplementary Material (ESI) for Nanoscale.

Supporting Information

Emerging electrospinning platform toward nanoparticle to single atoms transformation for steering selectivity in ammonia synthesis

Xuan Zheng[a], Jiace Hao [a], Zechao Zhuang [b], Qikang [c], Xiaofan Wang[a], Shuanglong Lu [a], Fang Duan [a], Mingliang Du[*a] and Han Zhu[*a]

a Key Laboratory of Synthetic and Biological Colloids, Ministry of Education, School of Chemical and Material Engineering, Jiangnan University, Wuxi 214122, China. Email: zhysw@jiangnan.edu.cn.

b Department of Chemical Engineering, Columbia University, New York, NY, 10027, USA.

c Institute of New Energy for Vehicles, School of Materials Science and Engineering, Tongji University, Shanghai, 201804 China

Experimental Section

Materials:

Tris(acetylacetonato)cobalt(III) ($C_{15}H_{21}CoO_6$,) and Ammonium sulfate-^{15}N ($(^{15}NH_4)_2SO_4$) were both provided by Shanghai Aladdin Reagent Co., Ltd. Potassium nitrate (KNO_3), potassium nitrite (KNO_2), sodium hydroxide (NaOH), N-(1-naphthyl) ethylenediamine dihydrochloride, sulfanilamide, Potassium sulfate (K_2SO_4), phosphoric acid (H_3PO_4), Salicylic acid, Ammonium chloride (NH_4Cl), sodium citrate dihydrate, hydrochloric acid (HCl) and ethanol (C_2H_5OH) were purchased from Sinopharm Chemical Reagent Co., Ltd. Sodium Hypochlorite Pentahydrate ($NaClO{\cdot}5H_2O$), sodium nitroferricyanide dehydrate ($C_5FeN_6Na_2O{\cdot}2H_2O$) and potassium nitrate-$^{15}N$ ($K^{15}NO_3$) were purchased from Macklin Co., Ltd. Dimethyl sulfoxide (DMSO) was obtained from Cambridge Isotope Laboratories, Inc. 4-Dimethylaminobenzaldehyde ($C_9H_{11}NO$) was acquired by Sigma-Aldrich. Argon (Ar, 99.999 %) were bought from Xinxiyi Technology Co., Ltd. (Jiangsu, China). Ultrapure water was used to prepare the aqueous solution. All chemicals were analytical grades.

Synthesis of Co SAs/CNFs and Co NPs/CNFs

Typically, $C_{15}H_{21}CoO_6$ (0.2 g) and polyvinyl pyrrolidone (PVP, 3 g) were dissolved in dimethyl Formamide (DMF) (16 g) to obtain homogeneous solution after 6 h magnetic stirring at room temperature. Electrospinning experiments were performed at an anode voltage of 20 kV with an injection rate of 0.4 mL h^{-1}. Then the obtained $Co(C_5H_7O_2)_2$/PVP precursor nanofibers were pre-oxidized in an oven at 220 °C for 6 h under ambient atmosphere. It was then transferred to a chemical vapor deposition (CVD) furnace for carbonization at 800°C with a heating rate of 5°C min^{-1} and kept in an argon atmosphere for 3 h. After the temperature dropped to room temperature, the temperature was again raised to 1000°C at a heating rate of 5°C min^{-1} for carbonization and maintained in a H_2/Ar atmosphere (1:9) for 0.5 h. Finally, the as-synthesized Co SAs/CNFs was obtained. In addition, the Co NPs/CNFs and Co SAs-Co NPs/CNFs prepared at different graphitization temperatures (800 and 900 °C).

Materials Characterizations

The morphology of the as-prepared catalysts was investigated by scanning electron microscopy (SEM) and transmission electron microscopy (TEM). SEM was conducted on Hitachi S-4800 FE-SEM with an acceleration voltage of 5 kV and a current of 10 μA. TEM, high-angle annular dark-field scanning transmission electron microscopy (HAADF-STEM), and energy dispersive X-ray analysis were performed on a FEI Themis Z equipped with Cs corrector and energy-dispersive X-ray spectrometer at 200 kV. The XRD patterns of the catalysts were collected on Bruker D8 Advance X-ray diffractometer. XPS was performed on Thermo Scientific Kα system with the C 1s peak (284.8 eV) as reference. The element contents of the catalysts were measured on PerkinElmer Avio 200 inductively coupled plasma optical emission spectroscopy (ICP-OES). The Invia microscope Raman spectrometer with a 532 nm excitation source is provided by Renishaw (Shanghai) Trading Company Ltd. The differential electrochemical mass spectrometry (DEMS) is provided by Linglu instruments (Shanghai) Co. Ltd to perform online analysis of produced intermediates and products. 1H NMR is performed on the 600 M Bruker AVANCE III HD. The ultraviolet-visible (UV-Vis) absorbance spectra are measured on PERSEE TU-1950. The X-ray absorption spectra of the catalysts at Co K-edge was recorded at on beamline 12-BM in the Advanced Photon Source at Argonne National Laboratory in a transmission mode. Co foil and CoO were used as references. The acquired Extended EXAFS and X-ray absorption near-edge structure (XANES) data reduction and analysis were analyzed by Athena and Artemis software. For Wavelet Transform analysis, the χ(k) exported from Athena was imported into the Hama Fortran code.

Electrochemical Measurements

The electrochemical measurements were performed in a customized H-type cell with two 40 mL hermetic compartments containing 40 mL Ar-saturated electrolyte (0.5 M KNO_3+0.1 M K_2SO_4, pH =8.2), cooperating with a CHI 760E electrochemical workstation. The sample was cut into 0.3 × 0.4 cm^{-2} as the working electrode, while graphite rod (99.999 %) and Ag/AgCl (3M KCl solution) were used as reference electrode and counter electrode, respectively. The average loading of Co SAs/CNFs is

about 0.2 mg cm^{-2}. A two-compartment cell was separated by the Nafion 211 membrane. The electrode potentials were converted to the reversible hydrogen electrode (RHE) by the following equation: $E_{RHE} = E_{Ag/AgCl} + 0.197\ V + 0.0591 \times pH$. The electrochemical cell was maintained in an Ar atmosphere during NO3RR tests. The linear sweep voltammetry (LSV) was performed at a rate of 5 mV s^{-1}. The tests were conducted at constant potentials (-0.8 V ~ -0.4 V vs. RHE) for 2 h. The electrochemical double-layer (C_{dl}) capacitances were calculated by cyclic voltammetry (CV) in a non-Faradic potential range with various scan rates from 5 to 100 mV s^{-1}.

Determination of ammonia

The concentration of ammonia product was spectrophotometrically detected by the standard indophenol blue indicator method. Briefly, 2 mL of the solution product, 2 mL of a 1 M NaOH solution with 5% salicylic acid and 5% sodium citrate, 1 mL of 0.05 M NaClO and 0.2 mL of 1% sodium nitroferricyanide (III) dihydrate ($C_5FeN_6Na_2O{\cdot}2H_2O$) solution were mixed. After standing in the dark for 2 h, the concentration of indophenol blue was detected by ultraviolet-visible (UV-Vis) spectrophotometer at a wavelength of 655 nm in the absorption spectrum. For the quantitative determination of the amount of NH_4^+, a standard NH_4Cl solution was used to calibrate the concentration-absorbance standard curve for a series of concentrations.

Determination of nitrite

Firstly, 0.2 g of N-(1-naphthyl) ethylenediamine dihydrochloride, 4 g of p-aminobenzenesulfonamide, and 10 mL of phosphoric acid (ρ = 1.685 g mL^{-1}) were added into 50 mL of deionized water and mixed thoroughly as the color reagent. When testing the electrolyte from electrolytic cell, it should be diluted to the detection range. Then 2 mL of the diluted electrolyte and 40 μL of color reagent were mixed together. After 20 min at room temperature, the absorption spectrum was measured by using a UV–vis spectrophotometer (UV2600), and the absorption intensity was recorded at a wavelength of 540 nm. A series of standard potassium nitrite solutions were used to obtain the concentration–absorbance curve by the same processes. To quantify the amount of NO2-, a calibration curve was built using standard KNO_2 solution (Figure S5).

Calculation of the FE_{NH4+} and $Yield_{NH4+}$.

$$Yield_{NH4+}\,(mmol\ h^{-1}\ cm^{-2}) = C_{NH4+} \times V / (18 \times t \times s) \quad (1)$$

$$FE_{NH4+}(\%) = (8 \times F \times C_{NH4+} \times V) \times (Q \times 18) \times 100\% \quad (2)$$

where V is the volume of electrolyte (40 mL); C_{NH4+} is the concentration of NH_4^+ (μg mL^{-1}); t is the reaction time (2 h); s is electrode area (cm^{-2}); F represents the Faraday constant (96485 C mol^{-1}); Q is the electric charge (C).

^{15}N and ^{14}N 1H-NMR measurements

First, a series of $^{15}NH_4^+$-^{15}N solutions ($(^{15}NH_4)_2SO_4$)) with known concentrations (0, 2.5, 5, 7.5,10, 15, μM) were prepared in 0.5 M K_2SO_4 as standards. The 500 μL of the $^{15}NH_4^+$-^{15}N standard solution with different concentrations was taken out, and 150 μL of 0.5 M H_2SO_4 solution was added to adjust the PH, and further quantified by 1H NMR at 400 MHz with external standards of DMSO (50 μL). The calibration was achieved using the peak area ratio between $^{15}NH_4^+$-^{15}N and DMSO, because the $^{15}NH_4^+$-^{15}N concentration and the area ratio were positively correlated. Similarly, the amount of $^{14}NH_4^+$-^{14}N was quantified by this method when $^{14}KNO_3$ was used as the feeding N-source. After electroreduction, the electrolyte was subjected to NMR quantitative analysis using the same method.

In-situ Raman spectroscopy

In-situ Raman spectroscopy was recorded on the above-mentioned Raman microscope under controlled potentials by electrochemical workstation. The operando electrochemical Raman test was carried out in a round home-made electrolyzer. A platinum wire and Ag/AgCl electrode were served as the counter and reference electrode, respectively. The in-situ Raman measurements were carried out over a range of 100 ~ 4000 cm^{-1} during the chronoamperometry measurements from 0 V to -1.1 V vs. RHE, and the dwell time at each potential was 5 min.

Differential electrochemical mass spectrometry (DEMS) measurements

Online DEMS experiments were performed to capture the molecular gas products formed during the urea synthesis reaction. In this part, Co SAs/CNFs electrocatalysts, Pt wire, and Ag/AgCl electrodes were used as the working electrode, the counter

electrode, and the reference electrode, respectively. Linear sweep voltammetry was performed within the range of -0.6 to -1.7 V vs. RHE at a scan rate of 6 mV s^{-1} until the baseline reached a stable state. After the electrochemical test was over and the mass signal returned to baseline, the next cycle was started. After five cycles, the experiment was ended.

DFT simulation

Spin-polarized density functional theory (DFT) calculations were carried out via Vienna ab initio simulation package (VASP) utilizing the projector augmented wave (PAW) potentials with a plane wave cutoff energy of 400 eV. The generalized gradient approximation (GGA) functional of Perdew, Burke, and Ernzerhof (PBE) was applied as the exchange-correlation functional. To prevent the interaction between two adjacent layers, a vacuum layer of 15 A were adopt for all the surface model. We employed a gamma-centered k-point grid to sample the Brillouin zones. The convergence criteria of electronic energies were 10^{-5} eV, and the atomic forces of 0.03 eV/A was adopt for all calculations.

To simulate the NO_3RR process on Co SAs/CNFs and Co NPs/CNFs catalysts, a p(5 × 5) supercell slab of graphene doped with 1 O atom and 1 Co atom (Co-C3O1) and a p(3 × 3) supercell slab of Co (100) surface were chosen as the DFT calculation models. 2×2×1 and 4×4×1 k-point meshes were used for Co-C3O1 and Co (100) models, respectively.

We used the computational hydrogen electrode (CHE) model proposed by Norskov to calculate the Gibbs free energy of NO_3RR elementary steps by the following equation:

$$\Delta G = \Delta E + \Delta ZPE - T\Delta S + Ue + \Delta G_{pH}$$

where ΔE, △ZPE, and △S are the DFT-calculated energy, the zero-point energy, and the entropy changes of the step. T represents the finite temperature, e is the elementary charge, U is the applied potential, and ΔG_{pH} is considered as the correction free energy of H+. The zero-point energy and the entropy change were calculated from vibrational frequencies.

The EXAFS signals fitting and wavelet transform (WT) analysis

The obtained XAFS data was processed in Athena (version 0.9.26) for background, pre-edge line and post-edge line calibrations. Then Fourier transformed fitting was carried out in Artemis (version 0.9.26) [1-2]. The k^3 weighting, k-range of ~3.0-~11.4 $Å^{-1}$ and R range of ~1.0-~3.0 Å were used for the fitting. The models of Co foil, CoO and sample were used to calculate the simulated scattering paths. The four parameters, coordination number, bond length, Debye-Waller factor and E0 shift (CN, R, σ^2, ΔE_0) were fitted and partially fixed. For Wavelet Transform analysis, the $\chi(k)$ exported from Athena was imported into the Hama Fortran code[3]. The parameters were listed as follow: R range, 0 - 3 Å, k range, 3- 13.9 $Å^{-1}$; k weight, 3; and Morlet function with $\kappa=5$, $\sigma=1$ was used as the mother wavelet to provide the overall distribution.

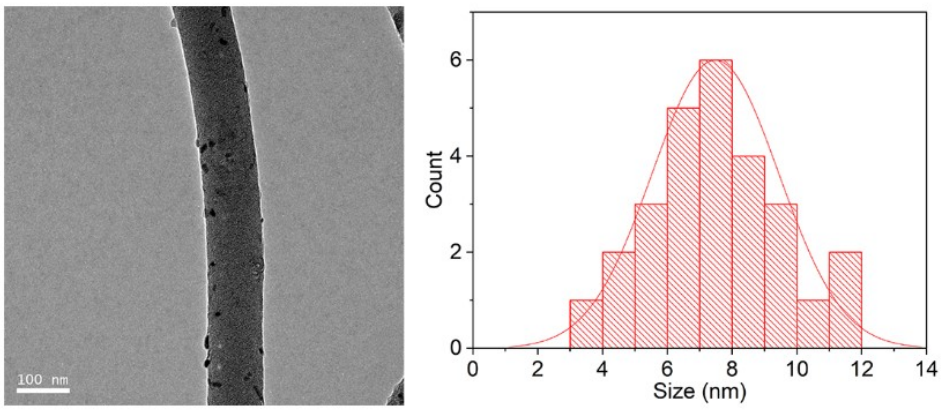

Figure S1. TEM image and nanoparticle size distribution profile of Co NPs/CNFs.

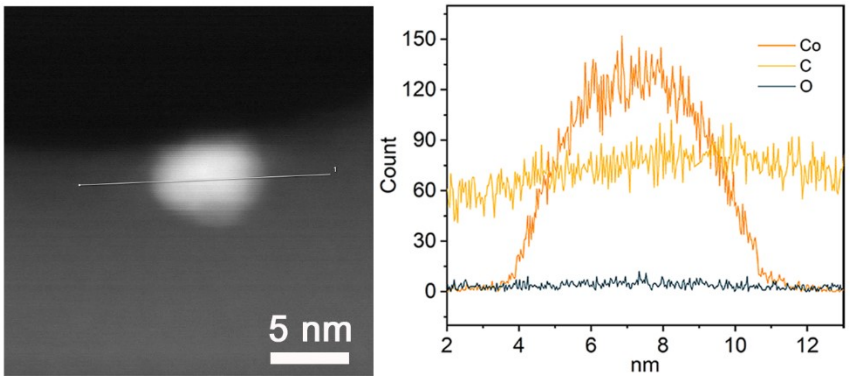

Figure S2. Line-scan EDX spectra of Co NPs/CNFs.

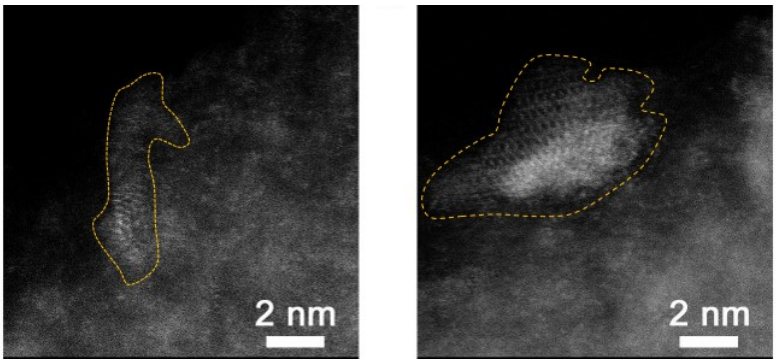

Figure S3. Aberration-corrected HAADF-STEM image containing the coexistence of Co SAs and Co NPs prepared at 900 °C

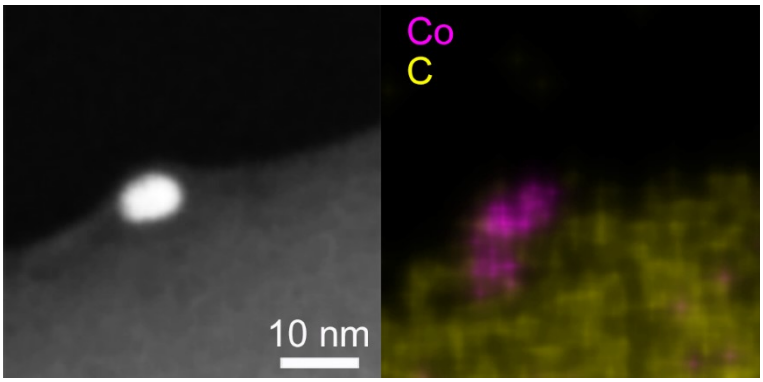

Figure S4. High-magnification STEM-EDS mapping images containing the coexistence of Co SAs and Co NPs prepared at 900 °C

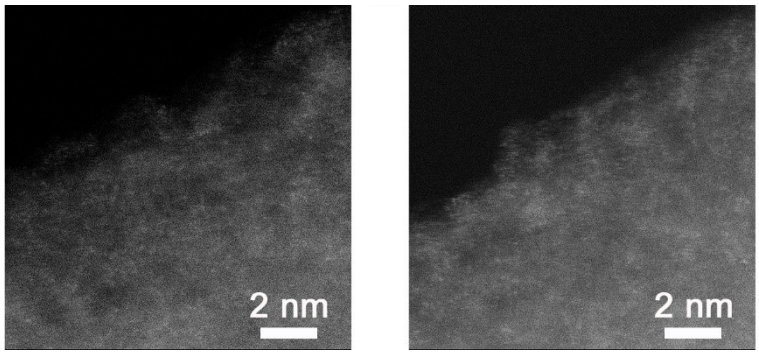

Figure S5. Aberration-corrected HAADF-STEM image of Co SAs/CNFs.

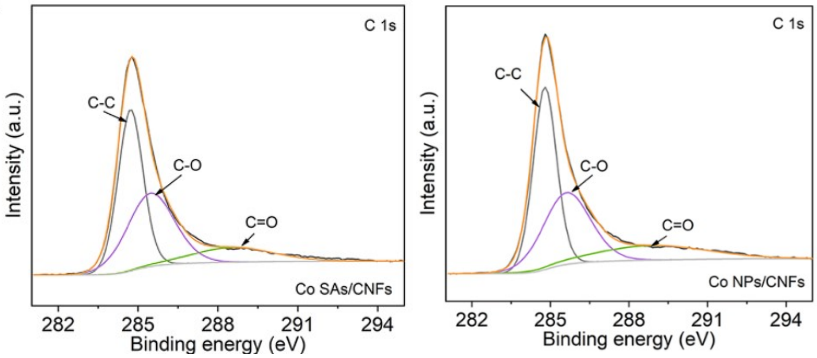

Figure S6. C 1s XPS spectra of Co SAs/CNFs and Co NPs/CNFs.

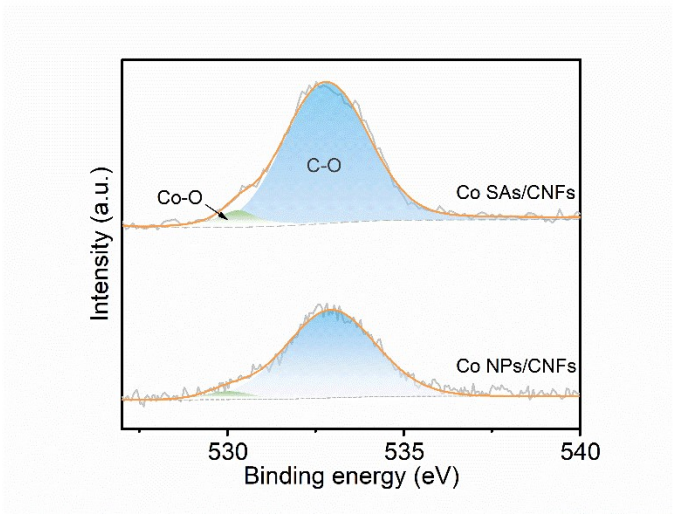

Figure S7. XPS spectra of the O 1s for Co SAs/CNFs and Co NPs/CNFs.

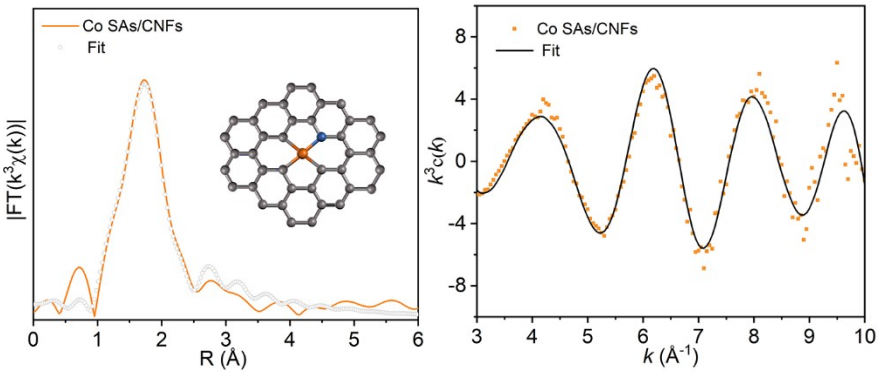

Figure S8. (a) Co K-edge EXAFS fitting analysis of Co SAs/CNFs in R space and d) k space.

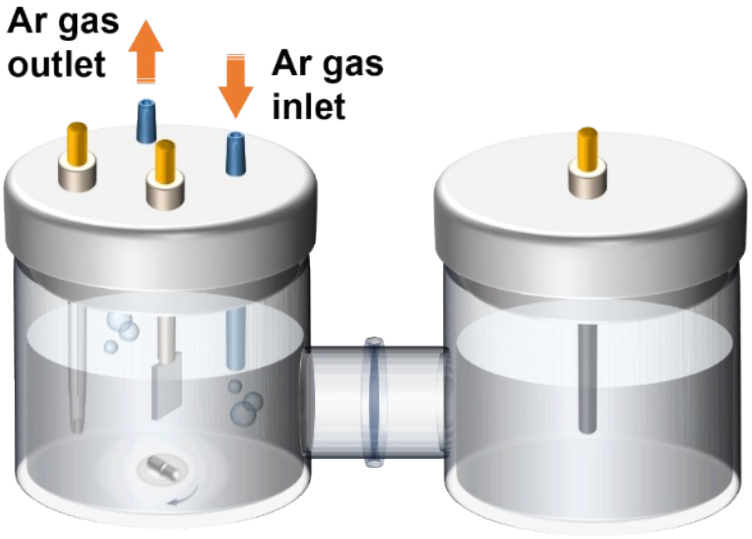

Figure S9. Schematic diagram of the H-type cell (H-cell) for NH_4^+ synthesis.

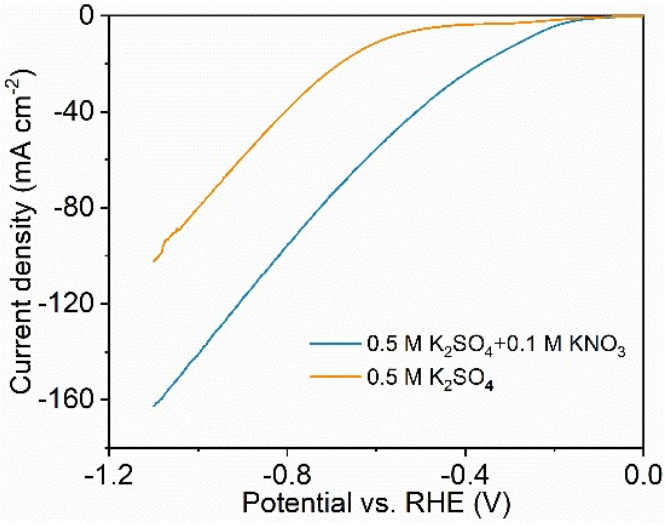

Figure S10. LSV curves of Co SAs/CNFs in 0.1 M K_2SO_4 with and without 0.1 M KNO_3.

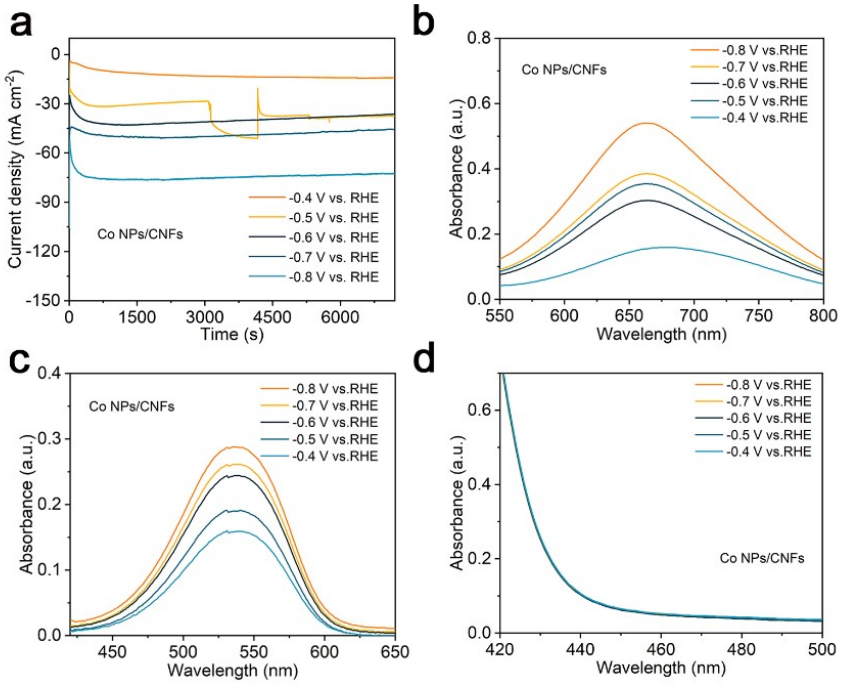

Figure S11. (a) Chronoamperometry curves of Co NPs/CNFs at various potentials for 2 h in Ar-saturated 0.5 M K_2SO_4 and 0.1 M KNO_3. (b) UV-Vis absorption spectra of NH_4^+ after 2 h electrolysis of Co SAs/CNFs at various potentials (diluted 40 times). (c) UV-Vis absorption spectra of NO_2^- after 2 h electrolysis of Co NPs/CNFs at various potentials (diluted 20 times). (d) UV-Vis absorption spectra of N_2H_4 after 2 h electrolysis of Co NPs/CNFs at various potentials.

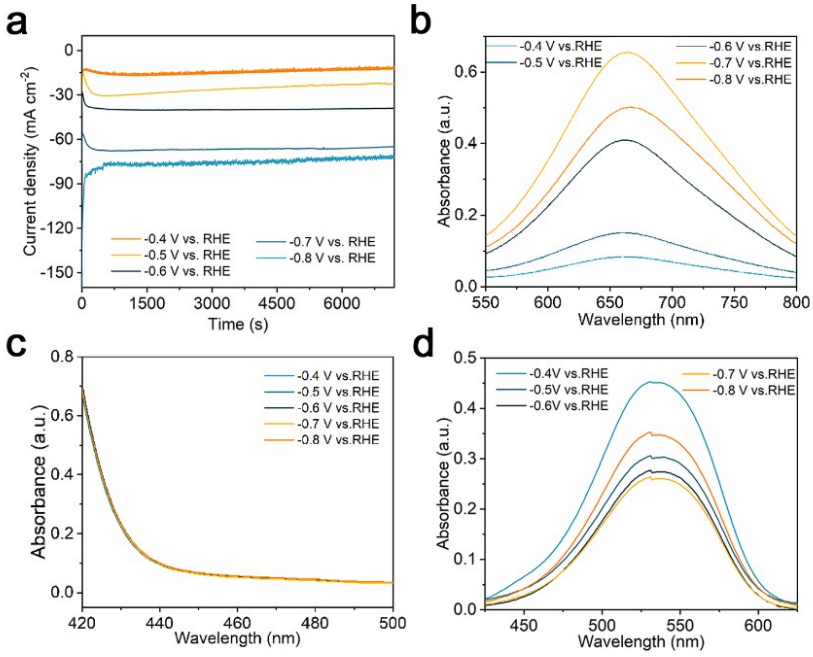

Figure S12. (a) Chronoamperometry curves of Co SAs/CNFs at various potentials for 2 h in Ar-saturated 0.5 M K_2SO_4 and 0.1 M KNO_3. (b) UV-Vis absorption spectra of NH_4^+ after 2 h electrolysis

of Co SAs/CNFs at various potentials (diluted 40 times). (c) UV-Vis absorption spectra of N_2H_4 after 2 h electrolysis of CNFs at various potentials. (d) UV-VIS absorption spectra of NO_2^- after 2 h electrolysis of Co SAs/CNFs at various potentials (diluted 20 times).

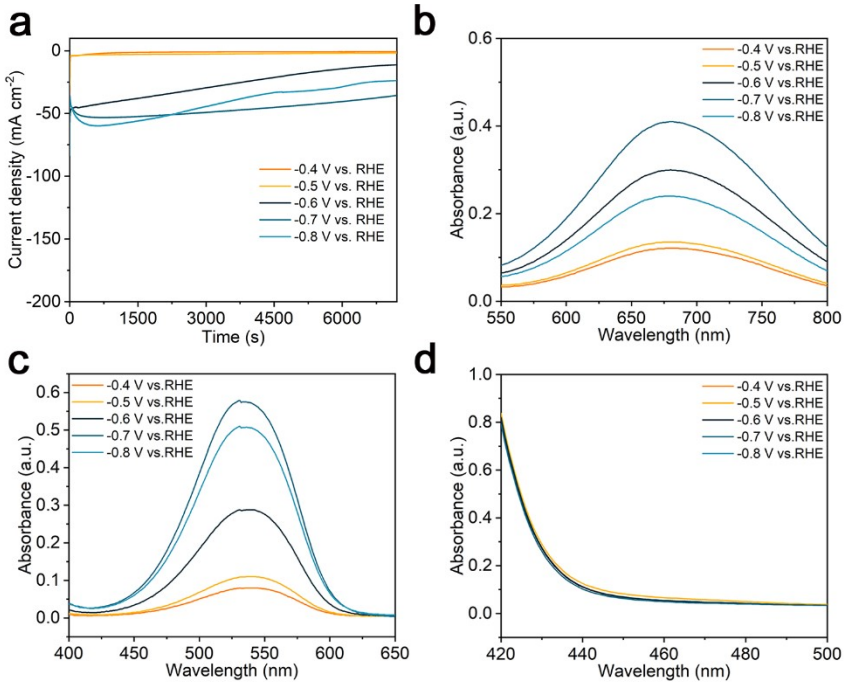

Figure S13. (a) Chronoamperometry curves of CNFs at various potentials for 2 h in Ar-saturated 0.5 M K_2SO_4 and 0.1 M KNO_3. (b) UV-Vis absorption spectra of NH_4^+ after 2 h electrolysis of CNFs at various potentials (diluted 40 times). (c) UV-Vis absorption spectra of NO_2^- after 2 h electrolysis of CNFs at various potentials (diluted 20 times). (d) UV-Vis absorption spectra of N_2H_4 after 2 h electrolysis of CNFs at various potentials.

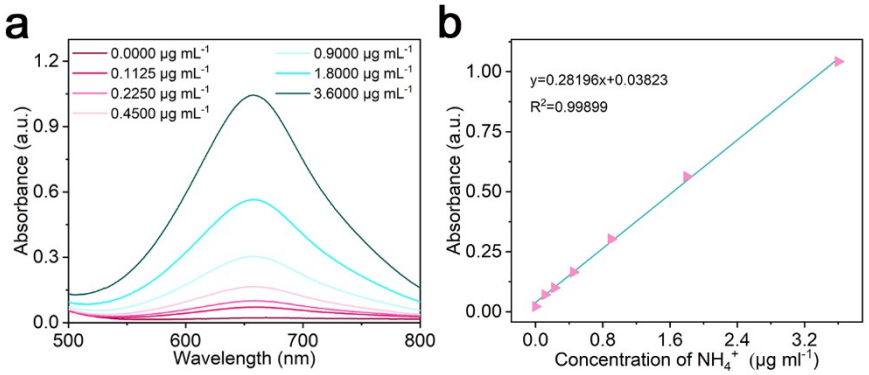

Figure S14. (a) UV-Vis absorption spectra of indophenol assays with NH_4^+ ions after incubated for 2 h at room temperature. (b) The calibration curve used for estimation of NH_4^+.

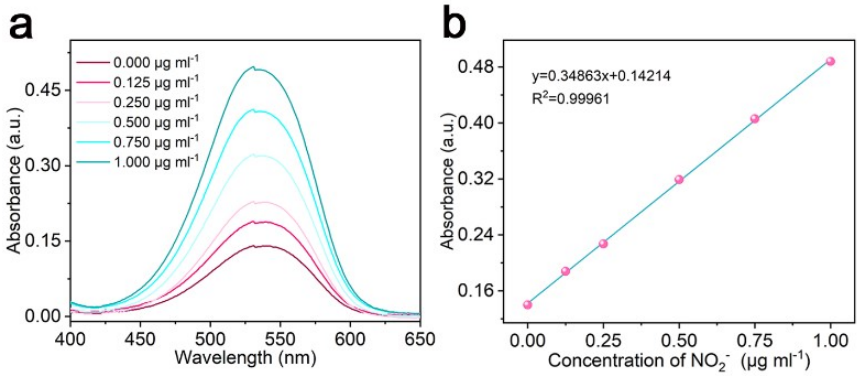

Figure S15. (a) UV-Vis absorption spectra of various NO_2^- concentrations at room temperature. (b) The calibration curve used for estimation of NO_2^-.

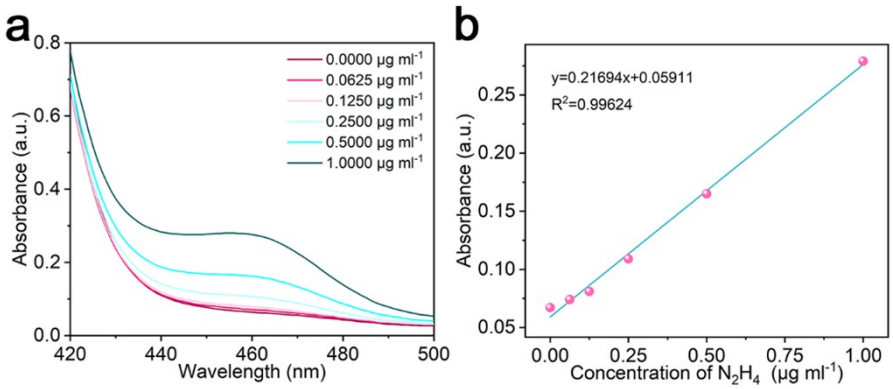

Figure S16. (a) UV-Vis absorption spectra of various N_2H_4 concentrations at room temperature. (b) The calibration curve used for estimation of N_2H_4.

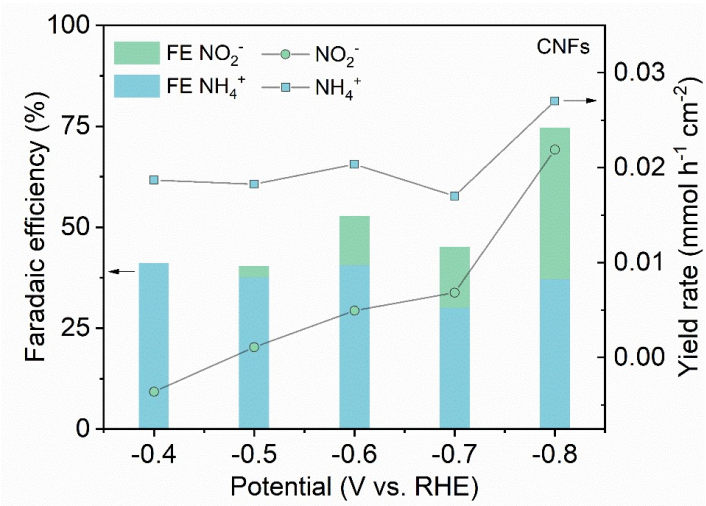

Figure S17. The yields and FEs of different products (NH_4^+, NO_2^-) at various potentials for CNFs.

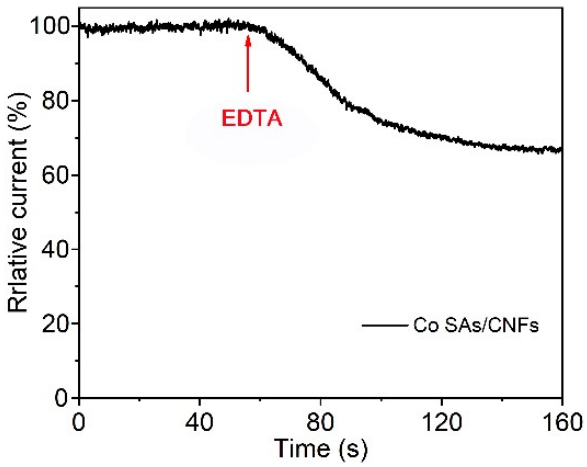

Figure S18. Poisoning experiment for electrochemical nitrate reduction of Co SAs/CNFs.

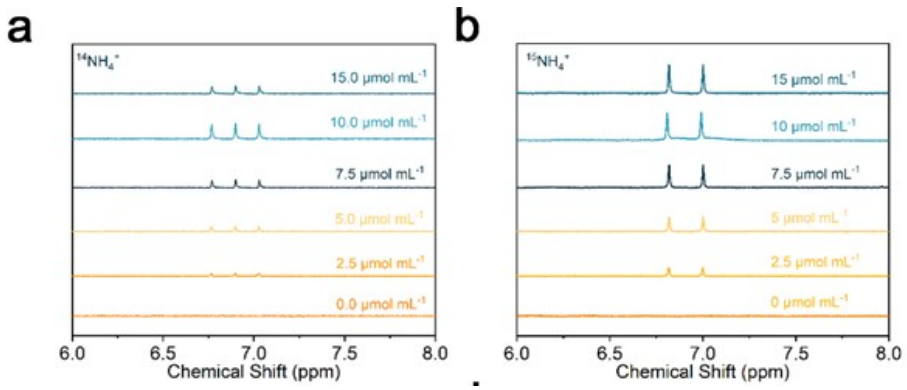

Figure S19. ^{1}H NMR spectra (400 MHz) of (a) $^{14}NH_4^+$-^{14}N and (b) $^{15}NH_4^+$-^{15}N with different concentrations.

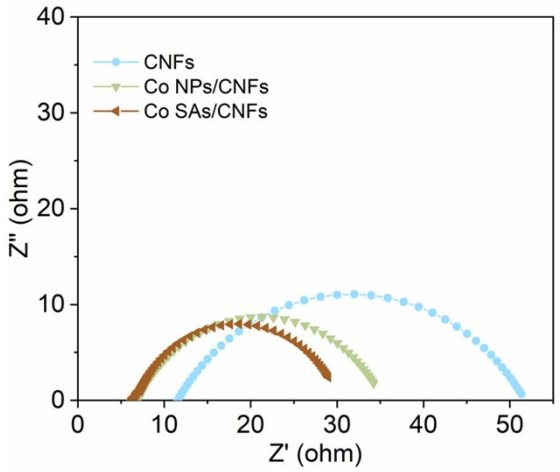

Figure S20. Electrochemical impedance spectra of CNFs, Co NPs/CNFs and Co SAs/CNFs.

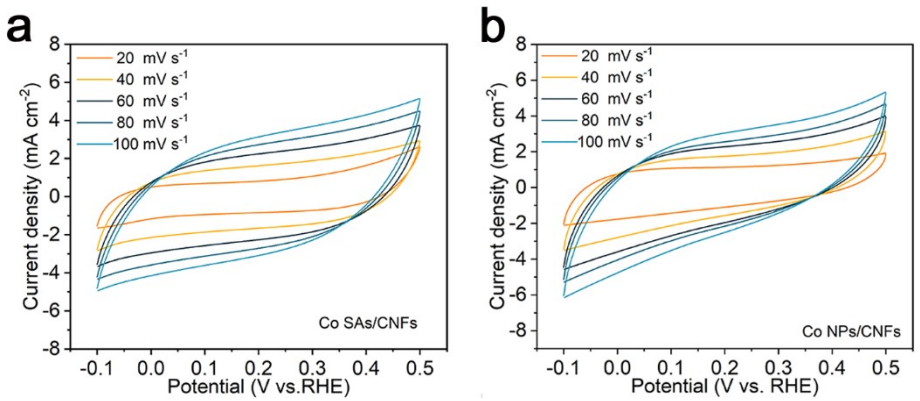

Figure S21. Cyclic voltammograms of (a) Co SAs/CNFs (b) and Co NPs/CNFs in an Ar saturated 0.1 M KNO_3 0.5 M K_2SO_4 electrolyte.

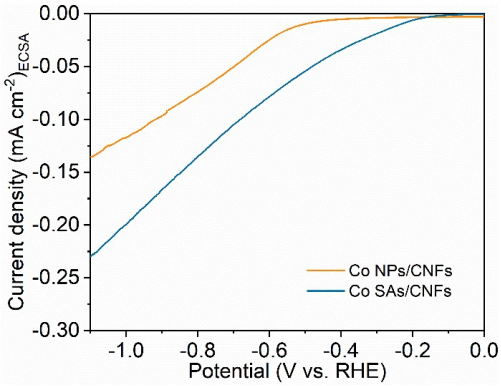

Figure S22. The LSV curves of Co NPs/CNFs and Co SAs/CNFs normalized by the electrochemical active surface area (ECSA).

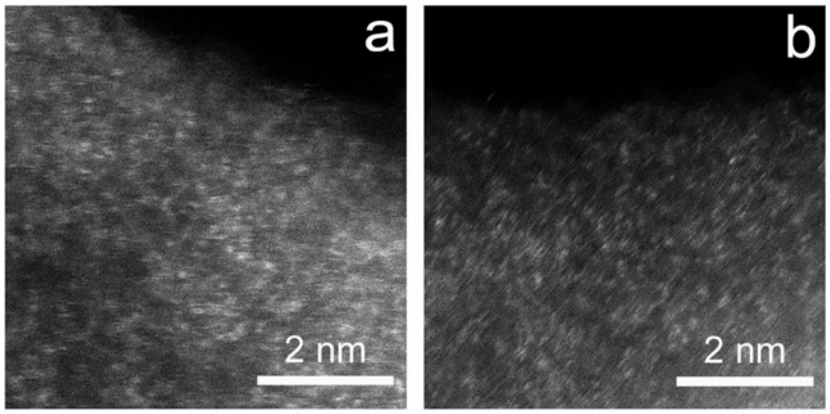

Figure S23. Atomic-scale HAADF-STEM images of the Co SAs/CNFs after the long-term stability tests.

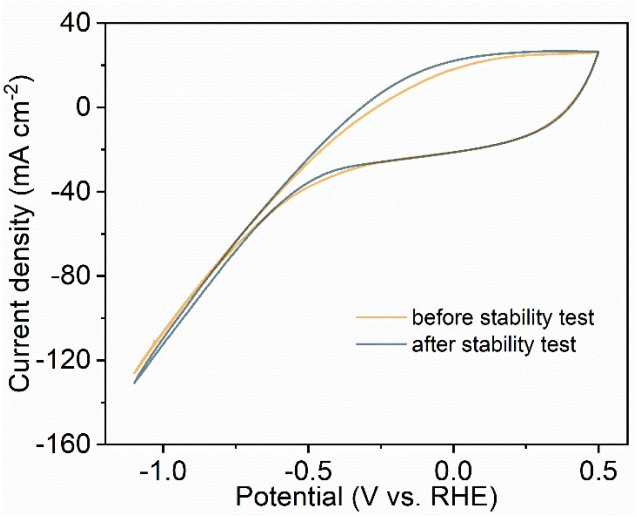

Figure S24. CV curves of Co SAs/CNFs before and after long-term stability tests.

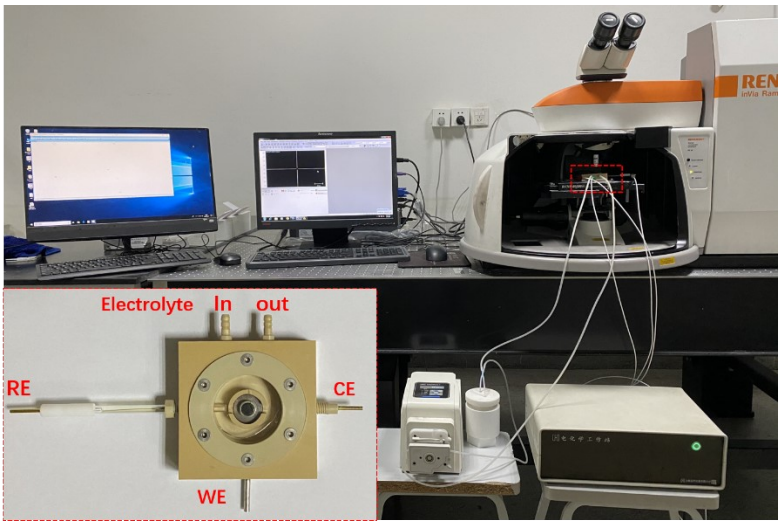

Figure S25. The optical image of instrument for in-situ electrochemical Raman spectroscopy characterization.

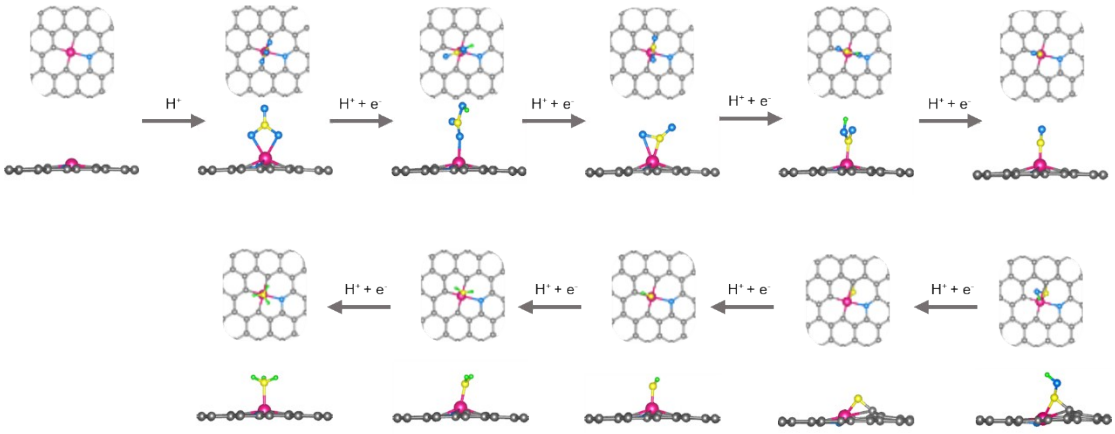

Figure S26. Structural models of Co SAs/CNFs during NO_3RR in this work. Co pink, C gray, N yellow, O blue and H green atoms.

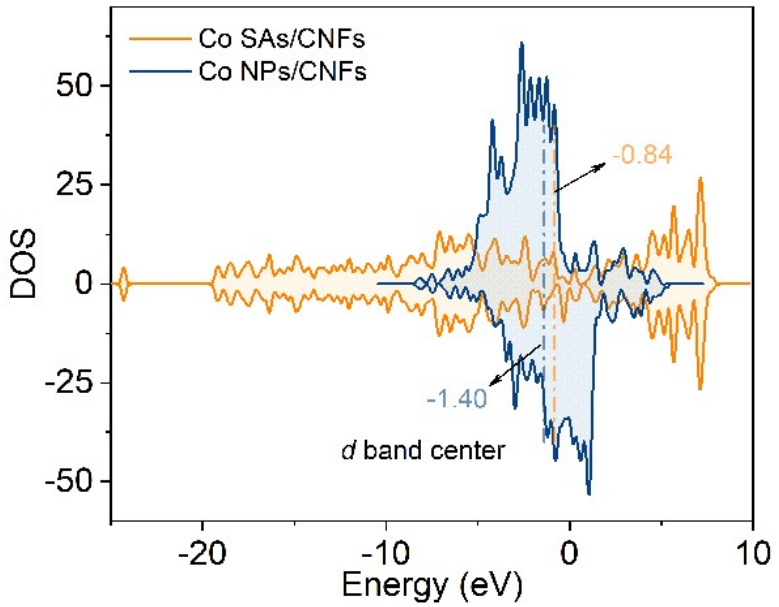

Figure S27. The calculated DOS of Co SAs/CNFs and Co NPs/CNFs models.

Table S1. Metal content of the Co SAs/CNFs and Co NPs/CNFs determined by ICP-AES.

Sample	ICP-OES analysis (wt. %)
Co SAs/CNFs	0.37
Co NPs/CNFs	0.32

Table S2. EXAFS fitting parameters at the Co K-edge for various samples. (S_0^2=1.0)

Sample	Path	N[a]	R(Å)[b]	σ^2(Å^2)[c]	ΔE_0(eV)[d]	R factor
Co foil	Co-Co	12.00	2.49 (±0.01)	0.0063 (±0.0003)	6.98 (±0.35)	0.0012
CoO	Co-Co	6.00	2.13 (±0.01)	0.0090 (±0.0006)	-1.35 (±1.23)	0.0017
	Co-O	12.00	3.01 (±0.01)	0.0090 (±0.0006)	-1.35 (±1.23)	
Sample	Co-C	2.89	2.07 (±0.02)	0.0051 (±0.0006)	8.81 (±1.46)	0.0057
	Co-O	1.07	1.96 (±0.02)	0.0099 (±0.0015)	8.13 (±3.23)	

[a]CN, coordination number; [b]R, distance between absorber and backscatter atoms; [c]σ^2, Debye-Waller factor to account for both thermal and structural disorders; [d]ΔE_0, inner potential correction; R factor indicates the goodness of the fit. According to the experimental EXAFS fit of Co foil by fixing CN as the known crystallographic value. Fitting range: 3.0≤k (/Å) ≤ 12.0 and 1.0 ≤ R (Å) ≤ 2.8 (Co foil).; 3.0≤k (/Å) ≤ 11.5 and 1.2 ≤ R (Å) ≤ 3.0(CoO).; 3.0≤k (/Å) ≤ 11.4 and 1.0 ≤ R (Å) ≤ 3.0 (Sample).

Table S3. The values of resistance in the fitted equivalent circuit of the Co SAs/CNFs and Co NPs/CNFs.

Elements	CNFs	Co NPs/CNFs	Co SAs/CNFs
Rs	11	8.9	6.5
Rct	37	27	18

Table S4. Comparison of performance of Co SAs/CNFs with reported catalysts by electrocatalytic nitrate reduction

Catalysts	Potential (V vs. RHE)	FE(%)	Yield rate (mmol h^{-1} cm^{-2})	Ref.
Co SAs/CNFs	-0.7	91.40	0.790	This work
v_{Co}-Co_3O_4/CC	-0.6	95.00	0.518	[1]
Co_3O_4/Co	-0.8	88.70	0.261	[2]
Co_3O_4-NS/Au-NWs	-0.5	97.76	0.082	[3]
SN Co-Li^+/PCNF	-0.94	90.20	0.710	[4]
Co_3O_4@NiO	-0.7	54.93	0.00693	[5]
$ZnCo_2O_4$	-0.6	80	0.0648	[6]
Fe SACs		75%	0.46	[7]
Co-CNP	-0.69	92	0.025	[8]
Fe-MoS_2	-0.48	98	0.03	[9]
BCN-Cu	-0.6	97.37	0.197	[10]
Cu/Ni-NC	-0.7	97.28	0.324	[11]
Cu SAAs	-0.7	77.7	0.0235	[12]
Cu@Th-BPYDC	-0.9	92.5	0.225	[13]
Fe–SA–N_2O_4	-0.68	92	0.541	[14]

References

1 Z. Q. Deng, C. Q. Ma, Z. R. Li, Y. S. Luo, L. C. Zhang, S. J. Sun, Q. Liu, J. Du, Q. P. Lu, B. Z. Zheng and X. P. Sun, High-Efficiency Electrochemical Nitrate Reduction to Ammonia on a Co_3O_4 Nanoarray Catalyst with Cobalt Vacancies, *ACS Appl. Mater. Interfaces*, 2022, 14 (41), 46595-46602.

2 F. L. Zhao, G. T. Hai, X. Li, Z. Y. Jiang and H. H. Wang, Enhanced electrocatalytic nitrate reduction to ammonia on cobalt oxide nanosheets via multiscale defect modulation, *Chem. Eng. J.*, 2023, 461, 141960.

3 Z. N. Zhang, Q. L Hong, X. H. Wang, H. Huang, S. N. Li and Y. Chen, Au Nanowires Decorated Ultrathin Co_3O_4 Nanosheets toward Light-Enhanced Nitrate Electroreduction, *Small*, 2023, 19, 2300530.

4 L. Mi, Q. Huo, J. Cao, X. Chen, H. Yang, Q. Hu and C. He, Achieving Synchronization of Electrochemical Production of Ammonia from Nitrate and Ammonia Capture by Constructing a “Two-In-One” Flow Cell Electrolyzer, *Adv. Energy Mater.*, 2022, 12, 2202247.

5 Y. T. Wang, C. B. Liu, B. Zhang and Y. F. Yu, Self-template synthesis of hierarchically structured Co_3O_4@NiO bifunctional electrodes for selective nitrate reduction and tetrahydroisoquinolines semi-dehydrogenation, *Sci. China Mater.*, 2020, 63(12): 2530-2538.

6 P. Huang, T. Fan, X. Ma, J. Zhang, Y. Zhang, Z. Chen and X. Yi, 3D Flower-Like Zinc Cobaltite for Electrocatalytic Reduction of Nitrate to Ammonia under Ambient Conditions, *ChemSusChem*, 2022, 63(12): 2530–2538.

7 Z. Y. Wu, M. Karamad and X. Yong, Electrochemical ammonia synthesis via nitrate reduction on Fe single atom catalyst, *Nat. Commun.*, 2021, 12, 2870.

8 J. Li, M. Li, N. An, S. Zhang, Q. Song, Y. Yang, J. Li, X. Liu, Boosted ammonium production by single cobalt atom catalysts with high Faradic efficiencies, *Proc. Natl. Acad. Sci. U. S. A.*, 2022, 119, e2123450119.

9 J. Li, Y. Zhan, C. Li, L. Zheng, E. Peti, K. Qi, Y. Zhan, H.Wu, W. Wang, A. Tiberj, X. Wang, M. Chhowalla, L. Lajaunie, R. Yu and D.Voiry, 3.4 % Solar-to-Ammonia

Efficiency from Nitrate Using Fe Single Atomic Catalyst Supported on MoS_2 Nanosheets, *Adv. Funct. Mater.*, 2022, 32, 2108316.

10 X. Zhao, X. Jia, Y. He, H. Zhang, X. Zhou, H. Zhang, S. Zhang, Y. Dong, X. Hu, A. V. Kuklin, G. V. Baryshnikov, H. Ågren and G. Hu, Two-dimensional BCN matrix inlaid with single-atom-Cu driven electrochemical nitrate reduction reaction to achieve sustainable industrial-grade production of ammonia, *Appl. Mater. Today*, 2021, 25, 101206.

11 Y. Wang, H. Yin, F. Dong, X. Zhao, Y. Qu, L. Wang, Y. Peng, D. Wang, W. Fang and J. Li, N-Coordinated Cu-Ni Dual-Single-Atom Catalyst for Highly Selective Electrocatalytic Reduction of Nitrate to Ammonia, Small, 2023, 19, 2207695.

12 P. Li, R. Li, Y. Liu, M. Xie, Z. Jin and G. Yu, Pulsed Nitrate-to-Ammonia Electroreduction Facilitated by Tandem Catalysis of Nitrite Intermediates, *J. Am. Chem. Soc.*, 2023, 145, 6471.

13 Z. Gao, Y. Lai, Y. Tao, L. Xiao, L. Zhang and F. Luo, Constructing Well-Defined and Robust Th-MOF-Supported Single Site Copper for Production and Storage of Ammonia from Electroreduction of Nitrate, *ACS Cent. Sci.*, 2021, 7, 1066.

14 W. D. Zhang, H. L. Dong and L. Zhou, Fe single-atom catalysts with pre-organized coordination structure for efficient electrochemical nitrate reduction to ammonia, *Appl. Catal. B*, 2022, 317, 121750.